Application of the Concave Arc Surface Collision Detection Method to Virtual Assembly

xin shi (xin_shi1@163.com)
Chongqing University
Li Tian
Chongqing University

Research Article

Keywords: Collision Detection, Concave Arc Surface Collision Detection, Motion Simulation, Parallel Groove Clamp

Posted Date: May 11th, 2021

DOI: https://doi.org/10.21203/rs.3.rs-504733/v1

Application of the Concave Arc Surface Collision Detection method to Virtual Assembly

Xin Shi*, Li Tian
School of Automation, Chongqing University, Chongqing, 400030 China
E-Mail: xin_shi1@163.com (*Corresponding author)

Abstract
Exact location calculation between each part of a parallel groove clamp when connecting a power line with a jumper is addressed in this paper. The relative location between a concave clamp and convex power line cannot be measured directly in live-line manipulation. We propose a concave arc surface collision detection method embedded in motion simulation. The relative location between irregular concave parts in the manipulation process can be obtained. The method is found to be computationally less expensive than convex partitioning collision detection techniques. This research provides a foundation for further study on robot hand manipulation with irregular assembly.

Key Words: Collision Detection, Concave Arc Surface Collision Detection, Motion Simulation, Parallel Groove Clamp

DECLARATIONS

-Ethical Approval

This work is in compliance with the ethical standards.

-Consent to Participate

No applicable

-Consent to Publish

The manuscript is approved by all authors for publication

-Authors Contributions

Xin Shi was in charge of investigation, validation, resources, project administration, supervision and funding acquisition. Li Tian was in charge of conceptualization, investigation, methodology, validation, and writing original draft.

-Funding

This work was supported by the National Natural Science Foundation of China (NSFC; grant number U1813216)

-Competing Interests

The authors declare no competing interests.

-Availability of data and materials

All data generated or analysed during this study are included in this published article

1. INTRODUCTION

Outage-free maintenance of electrical power lines is a basic demand in the electrical power industry. Parallel groove clamp manipulation, which is used in connecting a transmission line with a jumper, remains a dangerous procedure for line workers [1]. Therefore, it is inevitable a robotic worker to take the place of a human worker for switching on the jumper in live power line maintenance. Robotic applications for the maintenance of electrical live power lines began in the 1980s [2-3]. The current research directions are power transmission line inspection [4-5], teleoperation [6] and the development of mechanism design [7-8]. Robot technology plays an important role in solving this problem, but a robot cannot exactly mimic a person when manipulating the parallel groove clamp. Robotic hand and gripper designers have been interested in researching dexterous manipulation for many decades. However, robotic manipulation of rigid objects is still a problem that is worthy of further research. Liu et al. [9] developed a soft robotic gripper that can be used in grasping size-varied vulnerable objects. Vincent et al. [10] proposed a method for grasping objects lying on a flat surface. Bohg et al. [11] reviewed different methodologies for robot grasping. Wyk et al. [12] tested peg-in-hole manipulation control strategies. There have been many research efforts to examine the dexterity and robustness of robot grasping. To date, the grasping object has always been a single body or a part with little or no interaction with other objects (for example, the peg-in-hole task). It remains a challenging task to grasp or manipulate assemblies consisting of several parts.

Currently, research on assembly manipulation concentrates mainly on virtual assembly, and the main technologies are assembly sequences and collision detection [13-14]. Assembly sequence planning is an N-P hard combinatorial problem in which more than one objective function has to be optimized simultaneously to obtain a feasible sequence [15]. For the parallel groove clamp, the assembly sequence can be acquired by summarizing human operating experience due to the small number of parts. In addition, collision detection is always used for path planning in robotics. For assembly manipulation, the relative positions between each part can be calculated by collision detection. The collisions of parallel groove clamp manipulation occur mostly between power lines and splint grooves. However, convex bounding volumes are the main research objects for most collision detection methods [16]. The convex partitioning method is always used in the collision detection of concave volumes, which detects each object collision after dividing the objects into several pieces [17-18]. The disadvantage of the convex partitioning method is that the detail of edges is lost if the number of pieces is low; on the other hand, the computing time of collision detection grows as the number of pieces increases. Another common method for position detection is image detection. The spherical coordinate transform is always used for calculating the relative positions between each object [19]. The main disadvantage of image detection is that it cannot work in live environments.

Fortunately, Brozos-Vázquez et al. [20-21] provided a method to detect the positional relationship between ellipsoid and an elliptic paraboloid, which has inspired our work. Furthermore, the splint grooves in the parallel groove clamp can be considered an arc surface due to the design and product. Motivated by the above background, this paper examines a

new method of collision detection based on arc fitting. Then, the combined assembly sequence and the parts motion for parallel groove clamp manipulation are simulated. The clamping experiments show that the relative position between each part can be calculated accurately. The main contribution of this paper summaries as follow:

1. A new method for collision detection between a concave volume and a convex body is proposed.

2. The assembly sequence and position detection method supply a basis for further study of the parallel groove clamp.

3. A new robot solution for live power line maintenance is put forward.

2. ASSEMBLY SEQUENCE OF THE PARALLEL GROOVE CLAMP

To plan an assembly sequence, three factors must be considered: the part shapes, initial and final states, and connection relationships. Fig. 1 presents an exploded view of the parallel groove clamp and power lines, which consists of seven parts. For on-site operation, line workers do not start from the scattered state. The initial and final assembly states of the parallel groove clamp are shown in Fig. 2, which provides an anchor for assembly sequence planning.

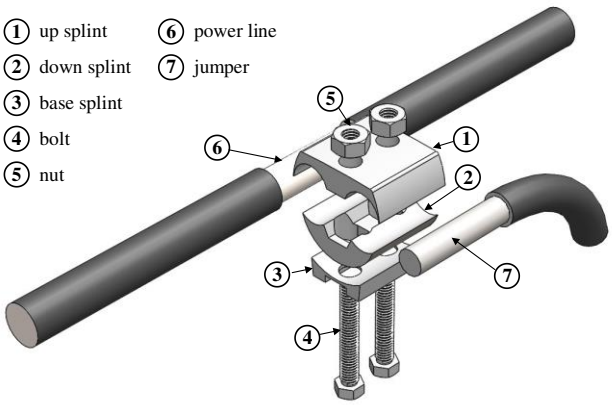

Fig. 1. Exploded view of the parallel groove clamp and power line.

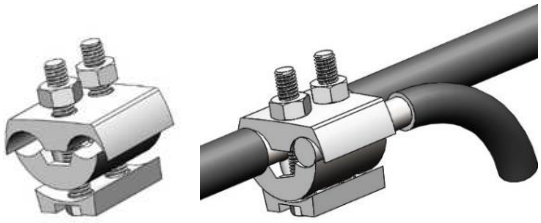

(a) (b)

Fig. 2. Assembly states of the parallel groove clamp. (a) Initial state; (b) final state.

The problem of assembly process planning can be regarded as permutations and combinations of motion of various parts [22]. The connection relationships provide constraint rules for these combinations. For parallel groove clamp manipulation, the connection relationships c_{ij} between P_i (ith part) and part P_j can be divided into four types:

$$c_{ij} = \begin{cases} 0, & P_i \text{ does not connect with part } P_j. \\ 1, & \text{screw joint} \\ 2, & \text{convex object collision} \\ 3, & \text{concave arc surface collision} \end{cases} \tag{1}$$

Then, the connection relationships matrix C in Fig. 2 (b) can be given by Eq. (1), as shown in Table 1 below.

Table 1. Connection relationship matrix C in the final state.

	P_1	P_2	P_3	P_4	P_5	P_6	P_7
P_1		0	0	2	2	3	3
P_2			3	2	0	3	3
P_3				2	0	0	0
P_4					1	0	0
P_5						0	0
P_6							0
P_7							

The assembly sequence planning of the parallel groove clamp does not require a complex algorithm due to a smaller number of parts. The assembly steps are reduced to four steps through a standard analysis of operation and the experience of line workers, as shown in Fig. 3.

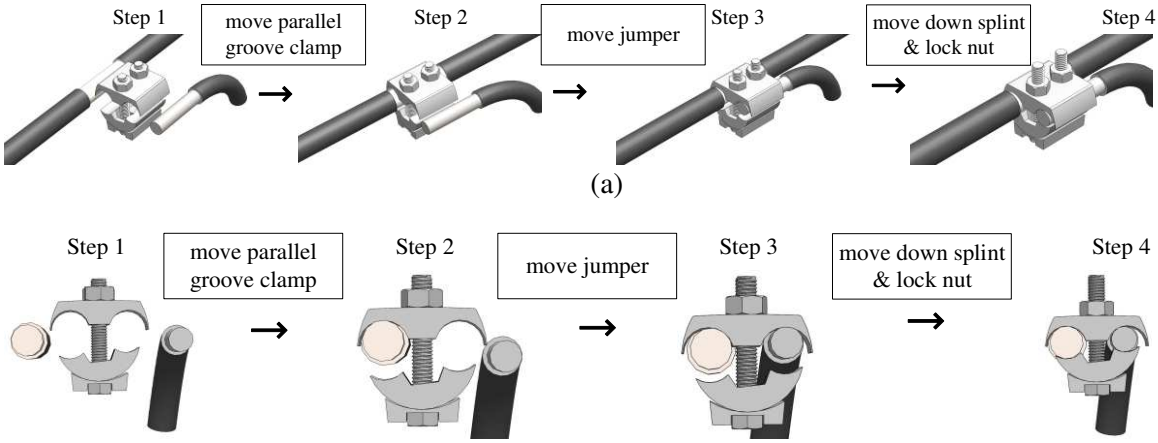

Fig. 3. Assembly steps. (a) 3D view; (b) cutaway view.

Grasping one part in the assembly leads other parts to follow. $P_i|P_j$ denotes that part P_j follows the movement of part P_i. Therefore, the assembly sequence in Fig. 3 is $P_1|P_2P_3P_4P_5 \rightarrow P_7 \rightarrow P_2 \rightarrow P_5|P_3P_4$.

3. CONCAVE ARC SURFACE COLLISION DETECTION

3.1. Collision Model Between Each Part

Because of assembly sequence constraints, there may be only one collision type or none between each pair of parts in the whole process. For the screw joint, the relative translation between the bolt and nut is achieved by screwing one of them. The scale factor between the rotation distance and translation distance is determined by the diameter and pitch.

For convex object collisions, the calculation of the distance between a point and the closest point on a plane or line segment is the basis of all detection algorithms. The collision detection method is based on an oriented bounding box (OBB) fit to detect these convex part collisions. A rectangular block is utilized as the oriented bounding. There are many possible representations for an OBB. For example, a centre point plus an orientation matrix and three

halfedge lengths are commonly the preferred representation for OBBs. The OBB-based collision detection method is used when the down splint collides with bolt, as shown in Fig. 4.

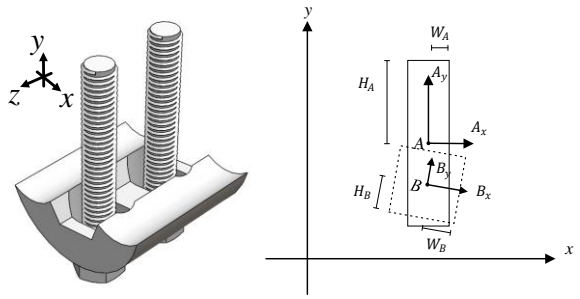

(a) (b)

Fig. 4. OBB-based collision detection. (a) Down splint collides with bolt; (b) simplified OBB collision.

The collision model between the down splint and bolt can be simplified as two rectangles due to the limitation of the relative motion along the $\pm z$-axis directions. The mathematical description of rectangle A is given as follows.

$$\begin{cases} P_A, & \text{centre point} \\ [A_x \quad A_y], & \text{orientation matrix} \\ H_A, W_A, & \text{halfedge extents along the axis} \end{cases} \tag{2}$$

There are four kinds of positional relationships between the down splint and bolt, as shown in Table 2 below.

Table 2. Four kinds of positional relationships for the down splint and bolt.

Positional relationship	**Legend**	**Mathematical description**
1) No collision	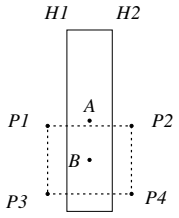	$\begin{cases} \mathrm{B_{p1_x}} < \mathrm{A_{H1_x}} \\ \mathrm{B_{p3_x}} < \mathrm{A_{H1_x}} \\ \mathrm{B_{p2_x}} > \mathrm{A_{H2_x}} \\ \mathrm{B_{p4_x}} > \mathrm{A_{H2_x}} \end{cases}$
2) One-point collision	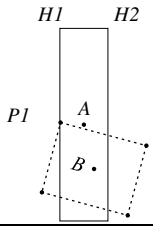	$\mathrm{B_{p1_x}} = \mathrm{A_{H1_x}}$ or $\mathrm{B_{p2_x}} = \mathrm{A_{H2_x}}$ or $\mathrm{B_{p3_x}} = \mathrm{A_{H1_x}}$ or $\mathrm{B_{p4_x}} = \mathrm{A_{H2_x}}$
3) Two-point collision on the same side	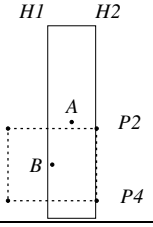	$\mathrm{B_{p1_x}} = \mathrm{B_{p3_x}} = \mathrm{A_{H1_x}}$ or $\mathrm{B_{p2_x}} = \mathrm{B_{p4_x}} = \mathrm{A_{H2_x}}$

4) Two-point collision on the diagonal	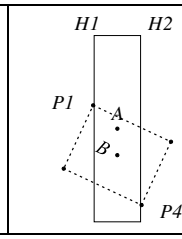	$\begin{cases} B_{p1_x} = A_{H1_x} \\ B_{p4_x} = A_{H2_x} \end{cases}$ or $\begin{cases} B_{p3_x} = A_{H1_x} \\ B_{p2_x} = A_{H2_x} \end{cases}$

*B_{p1_x} means the values on the x-axis of vertex $p1$ of rectangle B, and A_{H1_x} denotes the values on the x-axis of the left edge $H1$ of rectangle A.

The constraint of the bolt helps us acquire the motion track of the down splint, as listed in Table 2, although the starting and ending positions remain unknown. The down splint connects with the down splint when the up splint is grasped and leads the parallel groove clamp to move integrally. The grooves of the upper splint collide with the power line and jumper when the parallel groove clamp manipulation is completed. These collision methods can be regarded as collisions between the arc surface of the concave and convex cylinders. The cylinder can be regarded as the swept volume of a circle, and the arc surface can be regarded as the swept volume of an arc. Therefore, the starting and ending positions of the down splint can be calculated by distinguishing the position relationship between the arc and circle. In addition, collisions between the up splint and power lines are also acquired by this method.

3.2. Concave Arc Surface Collision Model

The Concave Arc Surface (CAS) collisions of the parallel groove clamp are beneficial for adapting different diameter sizes of power lines during manipulation. There are five CAS collisions during the parallel groove clamp manipulation process, as shown in Fig. 5.

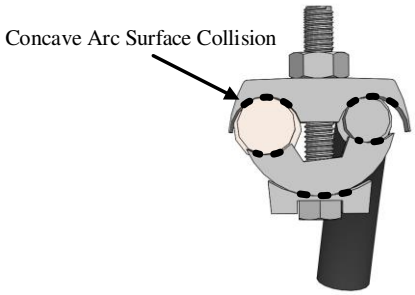

Fig. 5. CAS collision cutaway view.

Through the analysis above, the position model can be simplified into the position relationship between an arc $O_{\widehat{MN}}$ and a small circle O, as shown in Table 3. A small circle means that the radius of the circle is less than the radius of the arc.

Table 3. Positional relationship between arc and small circle.

	Inside	**Outside**	**Intersect**	**Exterior contact**	**Interior contact**
Major arc	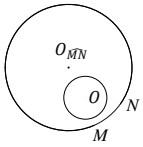	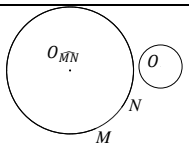	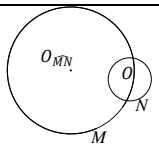	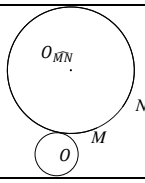	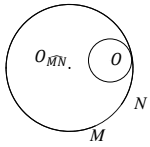

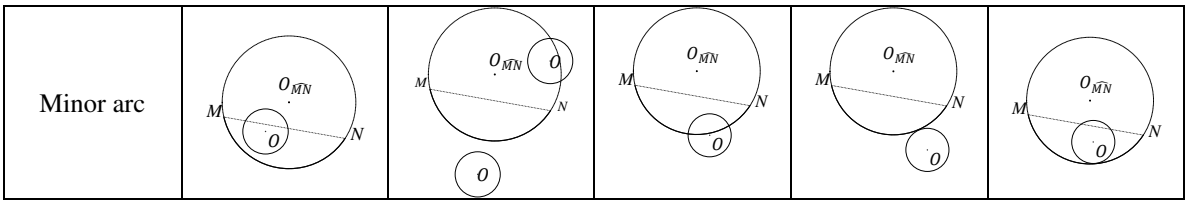

For Concave Arc Surface collision detection (CAS-CD), considering only the situation of minor arc fitting CAS, the mathematical description can be expressed as:

1) The small circle O is inside the area $\Gamma_{\widehat{MN}}$, which is enclosed by arc $O_{\widehat{MN}}$ and line segment MN:

$$\Gamma_{\widehat{MN}} \cap O \neq \emptyset \tag{3}$$

2) The small circle O is outside the area $\Gamma_{\widehat{MN}}$:

$$\Gamma_{\widehat{MN}} \cap O = \emptyset \tag{4}$$

3) The small circle O intersects arc $O_{\widehat{MN}}$:

$$d_{Op} < r_O \tag{5}$$

The distance d_{Op} between the centre point of the small circle O and the point p in arc $O_{\widehat{MN}}$ is less than the radius r_O of the small circle O.

4) The small circle O contacts arc $O_{\widehat{MN}}$, and there is only one cross point.

$$d_{Op} = r_O \tag{6}$$

4.1) The cross point is not the endpoint M or N in $O_{\widehat{MN}}$:

$$d_{O,\widehat{MN}} = \begin{cases} |r_o + r_{\widehat{MN}}|, & \text{exterior contact} \\ |r_o - r_{\widehat{MN}}|, & \text{interior contact} \end{cases} \tag{7}$$

4.2) The cross point is the endpoint M or N in $O_{\widehat{MN}}$. If the cross point is the endpoint M, draw a circle PRQ with centre M and radius r_O, join OM, and carry it through to the point P; the lines OM and circle PRQ intersect at Q. Draw RM from M perpendicular to OM. If the centre of the small circle O is located on arc $O_{\widehat{PR}}$, the small circle O contacts the exterior of arc $O_{\widehat{MN}}$, as shown in Fig. 6 (a). If the centre of the small circle O is located on arc $O_{\widehat{RQ}}$, the small circle O contacts the interior of arc $O_{\widehat{MN}}$, as shown in Fig. 6 (b).

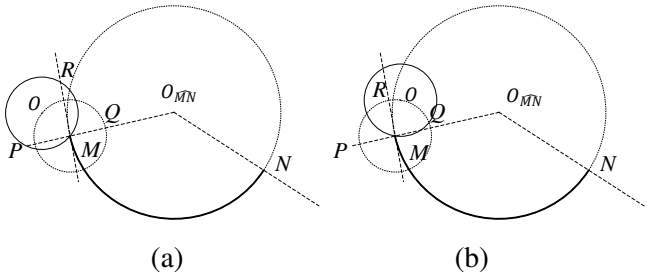

Fig. 6. The small circle O contacts arc $O_{\widehat{MN}}$ at point M. (a) Exterior contact; (b) interior contact.

4. SIMULATION AND DISCUSSION

4.1. Virtual Movement

The assembly sequence and CAS collision detection can be combined together in virtual movement if the physical structure of the parallel groove clamp transforms into a virtual simple model. Java 2D may help us complete this task through a virtual movement program.

Fig. 7 gives the flow diagram of the virtual movement algorithm of the parallel groove clamp. The final states remain the same regardless of whether the parallel groove clamp manipulation is accomplished by the robot, virtual simulation or line worker. Therefore, the absolute error of different part positions acquired in final states is a key index to verify this method. When the distance between the up splint and down splint is minimized in the assembly, the final state can be acquired. The final state of the virtual simulation based on CAS-CD is shown in Fig. 8 below.

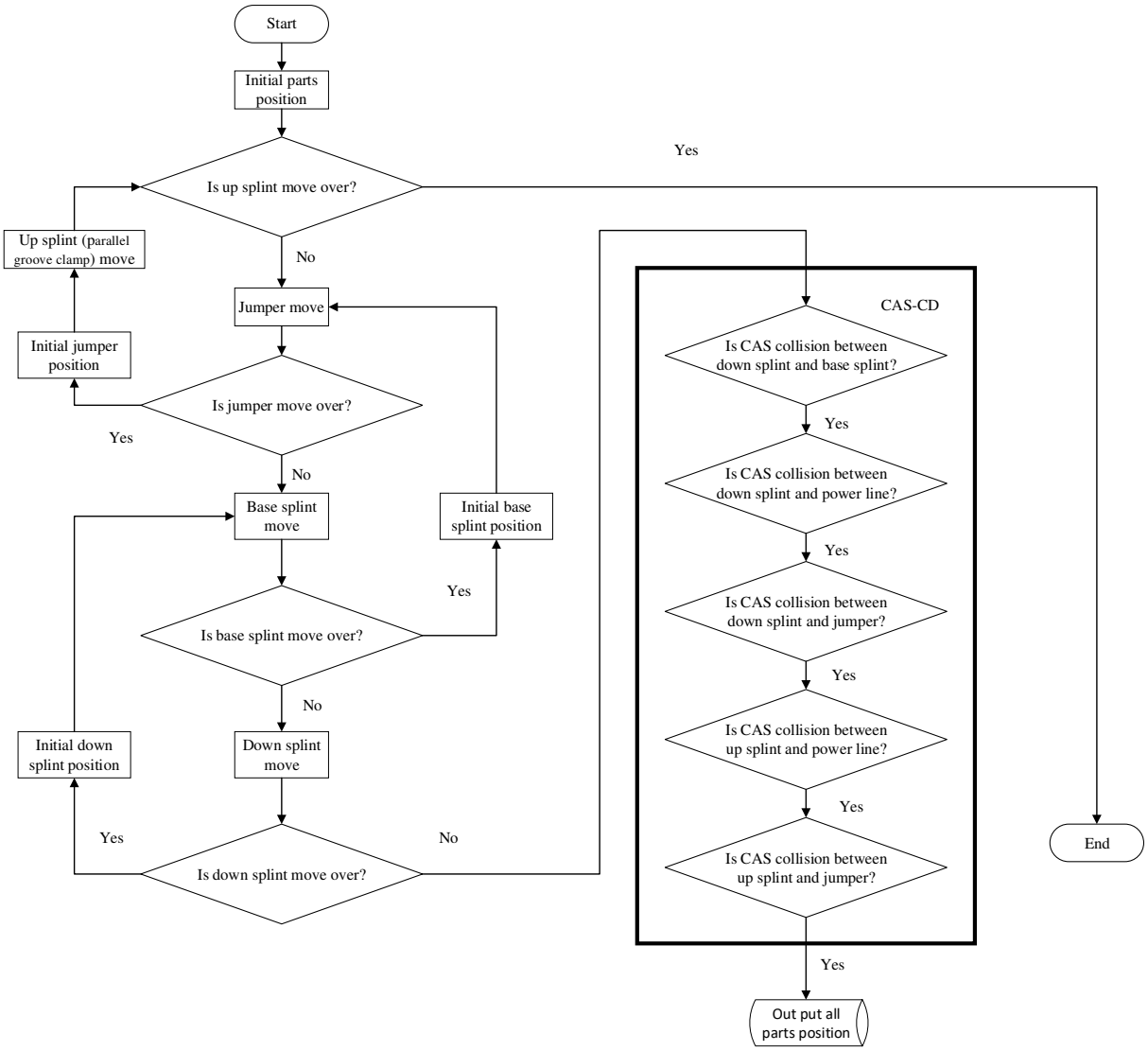

Fig. 7. Flow diagram of the virtual movement algorithm of the parallel groove clamp.

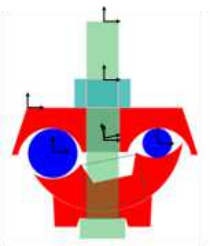

Fig. 8. Final state based on CAS-CD.

The transformational matrix ${}_{q}^{p}T = \begin{bmatrix} {}_{q}^{p}R & {}_{q}^{p}P \\ 0 & 1 \end{bmatrix}$ describes the relative position between each part. ${}_{q}^{p}R$ is the rotation matrix, and ${}_{q}^{p}P$ is the translation matrix. Hence, the location of part P_i is as follows: V_i is the location of part P_i, and V_j is the location of basic part P_j.

$$V_i = {}_{i}^{j}T \times V_j \tag{8}$$

In an actual scene, the position of the power line is constant, which is regarded as a reference frame. In Fig. 8, the transformational matrixes of other parts relative to the power line ⑥ are:

$${}_{1}^{6}T = \begin{bmatrix} 1 & 0 & -23.328 \\ 0 & 1 & -41.374 \\ 0 & 0 & 1 \end{bmatrix}, \quad {}_{2}^{6}T = \begin{bmatrix} 0.978 & -0.208 & 45.172 \\ 0.208 & 0.978 & -20.374 \\ 0 & 0 & 1 \end{bmatrix},$$

$${}_{3}^{6}T = \begin{bmatrix} 1 & 0 & 45.172 \\ 0 & 1 & -21.604 \\ 0 & 0 & 1 \end{bmatrix}, \quad {}_{4}^{6}T = \begin{bmatrix} 1 & 0 & 45.172 \\ 0 & 1 & -120.184 \\ 0 & 0 & 1 \end{bmatrix},$$

$${}_{5}^{6}T = \begin{bmatrix} 1 & 0 & 45.172 \\ 0 & 1 & -67.774 \\ 0 & 0 & 1 \end{bmatrix}, \quad {}_{7}^{6}T = \begin{bmatrix} 1 & 0 & 94.969 \\ 0 & 1 & -9.260 \\ 0 & 0 & 1 \end{bmatrix}.$$

4.2. Convex Partitioning and Image Detection

Polygons with ears are the typical method to divide concave polygons. The object with an arc is divided into many ears through the vertices on the arc [23]. The object of collision detection is the concave arc surface rather than every surface of the parallel groove clamp in the virtual simulation. Hence, the polygon ear method can be simplified in this situation, which divides the arc into a polyline. The unit radian α is used to describe the density of the polyline, and α is the radian of some arc that is replaced by a polyline. The collision detection between the polyline and circle represents the groove collision and power line, as shown in Fig. 9.

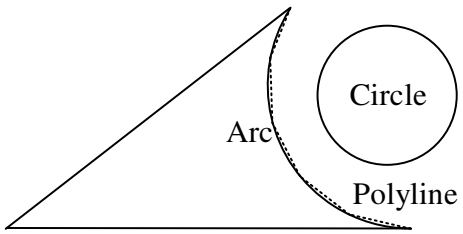

Fig. 9. Convex partition.

The core step of image detection is transforming the pixel distance to the physical distance [19]. The image detection method is shown in Fig. 10.

Fig. 10. Image detection.

The process is as follows:

1) Cutting two bare conductors: one is the transmission line, and the other is the jumper.
2) Inserting two bare conductors into the parallel groove clamp.
3) Fastening the nut through an electric wrench.
4) Using a camera to collect the image, which is the section of parallel groove clamp manipulation.
5) Labelling the end points of the parallel groove clamp in the image.
6) Calculating the pixel distance between each point.
7) Measuring the physical distance by a Vernier calliper.
8) Calculating the scale factor: the physical distance divides the pixel distance.
9) Calculating the real distance between the up splint and down splint.

4.3. Discussion

Through the analysis above, the absolute error about the position of each part can be simplified into a comparison with the distance between the up splint and down splint in the final state. The tightening torque is an index of the final state in the actual assembly. An electric wrench is used for tightening the nut, and the distance between the up splint and down splint is shown in Fig. 11.

Fig. 11. The actual distance.

We plug the sizes of the parallel groove clamp into the algorithm, which is shown in Fig. 7. The distance between the up splint and down splint in the final state can be found in the output data. Then, we replace the CAS-CD method with convex partitioning. By modifying the size of the unit radian, this distance in different densities of polylines can be acquired. Finally, the image detection method is repeated. The results are listed in Table 4.

Table 4. Distance between the up splint and down splint in the final state.

		Distance between the up splint and down splint (mm)	**Absolute error** (mm)
Actual distance		31.630	-
CAS-CD		31.530	0.100
Convex partitioning	$\alpha = 1^o$	31.863	0.233
	$\alpha = 5^o$	31.863	0.233
	$\alpha = 10^o$	31.863	0.233
	$\alpha = 20^o$	32.196	0.566
	$\alpha = 40^o$	32.863	1.233
Image detection		32.534	0.904
		33.672	2.042

	29.147	2.483
	32.450	0.820
	32.619	0.989

As shown in Table 4, the actual distance is greater than the distance acquired from the virtual motion based on the CAS-CD method. The main reason is that the cylinder cannot fit the power line. However, this is acceptable for parallel groove clamp manipulation because the absolute error is $0.1\,mm$. In the simulation of the convex partitioning method, the absolute errors are the same when $\alpha = 1^o, 5^o, 10^o$. This means that the absolute error remains constant within limits. When $\alpha = 10^o, 20^o, 40^o$, the absolute errors increase due to the loss of details on the groove surface. The absolute error of the convex partitioning method is higher than that of the CAS-CD method, which can better fit the groove surface. For image detection, the absolute errors are unstable due to the end points being marked manually. The absolute error from the CAS-CD method is lower than all results from image detection. The algorithm complexity is also an important indicator except for the absolute error of the object position, as shown in Table 5.

Table 5. Algorithm complexity.

	CAS-CD	**Convex Partitioning**	**Image Detection**
Part Motion	$M(n)$	$M(mn)$	-
Collision Detection	$C(1)$	$C(m)$	-
Time Complexity	$M(n^a) * C(b)$	$M(4m^{a-1}n^a) * C(bm)$	c

*a denotes the number of movement parts, and b denotes the number of groove surfaces. In addition, m denotes the numbers of line segments on a polyline that is used for fitting the arc, and c is a constant.

The algorithm complexity can be divided into two parts: part motion $M(n)$ and collision detection $C(1)$. For the CAS-CD method, the time complexity is $M(n^a) * C(b)$. For the convex partitioning method, the time complexity is $M(4m^{a-1}n^a) * C(bm)$. The time complexity of image detection is c. In general, the comparative results show that image detection is a fast method to calculate the parts' positions. However, this method is limited by the live environment, which precludes a cutaway view. The CAS-CD method has lower absolute error and time complexity than the convex partitioning method. Therefore, the CAS-CD method is more suitable for calculating the parts' positions during the process of parallel groove clamp manipulation.

5. CONCLUSION

The problem of grasping the parallel groove clamp by a robot hand, which is used for the maintenance of electrical live power lines, is analysed in this paper. We proposed a collision detection method based on CAS embedded in virtual assembly. This method is used to calculate the parts' positions during the process of parallel groove clamp manipulation. This method supplies a basis for further study of the parallel groove clamp. While no robot hand is used to verify this method, we have a much better understanding of robot design, which is used in parallel groove clamp manipulation. We plan to further study the grasp patterns and the mechanism in the future.

ACKNOWLEDGEMENTS

This work was supported by the National Natural Science Foundation of China (NSFC; grant number U1813216)

REFERENCES

[1] Power-Lines, E. IEEE Guide for Maintenance Methods on Energized Power-Lines. IEEE Standard 516, 2009, https://doi.org/10.1109/IEEESTD.2009.5137335
[2] Cohen, J. Live-line repair with Tomcat. EPRI Journal, 1987;5 14–19.
[3] Aracil R, Ferre M, Hernando M, Pinto E, Sebastian J M. Telerobotic system for live-power line maintenance: ROBTET. Control Eng Pract, 2002;10:11 1271-1281. https://doi.org/10.1016/S0967-0661(02)00182-X
[4] Nagarajan B, Li Y, Sun Z, Qin R. A routing algorithm for inspecting grid transmission system using suspended robot: Enhancing cost-effective and energy efficient infrastructure maintenance. J Clean Prod, 2019;219: 622-638. https://doi.org/10.1016/j.jclepro.2019.02.088
[5] Song Y, Wang H, Zhang J. A vision-based broken strand detection method for a power-line maintenance robot. IEEE T Power Deliver, 2014;29:5 2154-2161. https://doi.org/10.1109/TPWRD.2014.2328572
[6] Banthia V, Maddahi Y, Balakrishnan S, Sepehri, N. Haptic-enabled teleoperation of base-excited hydraulic manipulators applied to live-line maintenance. In: IEEE/RSJ International Conference on Intelligent Robots and Systems; Chicago, USA. 2014 p. 1222-1229. https://doi.org/10.1109/IROS.2014.6942713
[7] Jiang W, Yan Y, Zhang A, Yu L, Zuo G, Li H J, Chen W. Live maintenance robot for high-voltage transmission lines. Ind Robot, 2019;46:5 711-718. https://doi.org/10.1108/IR-03-2019-0057
[8] Scaff W, Hirakawa A R, Horikawa O. Non-conducting manipulator for live-line maintenance: Use of pneumatic artificial muscles. In: Proceedings of the 2014 3rd International Conference on Applied Robotics for the Power Industry; Foz do Iguassu, Brazil. 2014 p. 1-6. https://doi.org/10.1109/CARPI.2014.7030061
[9] Liu C H, Chen T L, Chiu C H, Hsu M C, Chen Y, Pai T Y, Peng W G, Chiang Y P. Optimal design of a soft robotic gripper for grasping unknown objects. Soft Robot, 2018;5:4 452-465. https://doi.org/10.1089/soro.2017.0121
[10] Babin V, St-Onge D, Gosselin C. Stable and repeatable grasping of flat objects on hard surfaces using passive and epicyclic mechanisms. Robot Cim-Int Manuf, 2019;55 1-10. https://doi.org/10.1016/j.rcim.2018.06.002
[11] Bohg J, Morales A, Asfour T, Kragic D. Data-driven grasp synthesis—a survey. IEEE T Robot, 2013;30:2 289-309. https://doi.org/10.1109/TRO.2013.2289018
[12] Van Wyk K, Culleton M, Falco J, Kelly K. Comparative peg-in-hole testing of a force-based manipulation controlled robotic hand. IEEE T Robot, 2018;34:2 542-549. https://doi.org/10.1109/TRO.2018.2791591
[13] Dogar M, Spielberg A, Baker S, Rus D. Multi-robot grasp planning for sequential assembly operations. Auton Robot, 2019,43:3 649-664. https://doi.org/10.1007/s10514-018-9748-z
[14] Maddahi Y, Zareinia K, Sepehri N. An augmented virtual fixture to improve task performance in robot-assisted live-line maintenance. Comput Electr Eng, 2015;43: 292-305. https://doi.org/10.1016/j.compeleceng.2014.07.006
[15] Murali G B, Deepak B B V L, Raju M V A, Biswal B B. Optimal robotic assembly sequence planning using stability graph through stable assembly subset identification. P I Mech Eng C-J Mec, 2019;233:15 5410-5430. https://doi.org/10.1177/0954406219842908
[16] Dinas S, Bañón J. M. A literature review of bounding volumes hierarchy focused on collision detection. Ingeniería y competitividad, 2015;17:1 49-62. https://doi.org/10.25100/iyc.v17i1.2200
[17] Wang H R, Liu J, Liu X L. The honeycomb-shaped spatial decomposition collision detection algorithm. In: International Conference on Machine Learning and Cybernetics, 2009;3 p. 1861-1865. https://doi.org/10.1109/ICMLC.2009.5212253
[18] Chowriappa A, Wirz R, Ashammagari A R, Kesavadas T. A convex decomposition methodology for collision detection, In: IEEE Virtual Reality (VR), 2013 p. 57-58, https://doi.org/10.1109/VR.2013.6549361
[19] Luo L, Mo J, Yang X. A method of using image-view pairs to represent complex 3D objects, Cogent Engineering, 2018;5:1. https://doi.org/10.1080/23311916.2018.1491264
[20] Brozos-Vázquez M, Pereira-Sáez M J, Souto-Salorio M J, Tarrío-Tobar A D. Classification of the relative positions between a small ellipsoid and an elliptic paraboloid. Comput Aided Geom D, 2019;72 34-48. https://doi.org/10.1016/j.cagd.2019.05.002

[21] Brozos-Vázquez M, Pereira-Sáez M J, Souto-Salorio M J, Tarrío-Tobar A D. Classification of the relative positions between a circular hyperboloid of one sheet and a sphere. Math Method Appl Sci, 2018;41:13 5274-5292. https://doi.org/10.1002/mma.5079
[22] Bahubalendruni M R, Gulivindala A K, Varupala S P, Palavalasa D K. Optimal Assembly Sequence generation through computational approach. Sādhanā, 2019;44:8 1-9, https://doi.org/10.1007/s12046-019-1157-2
[23] Meisters G H. Polygons have ears. The American Mathematical Monthly, 1975;82:6 648-651, https://doi.org/10.1080/00029890.1975.11993898

Figures

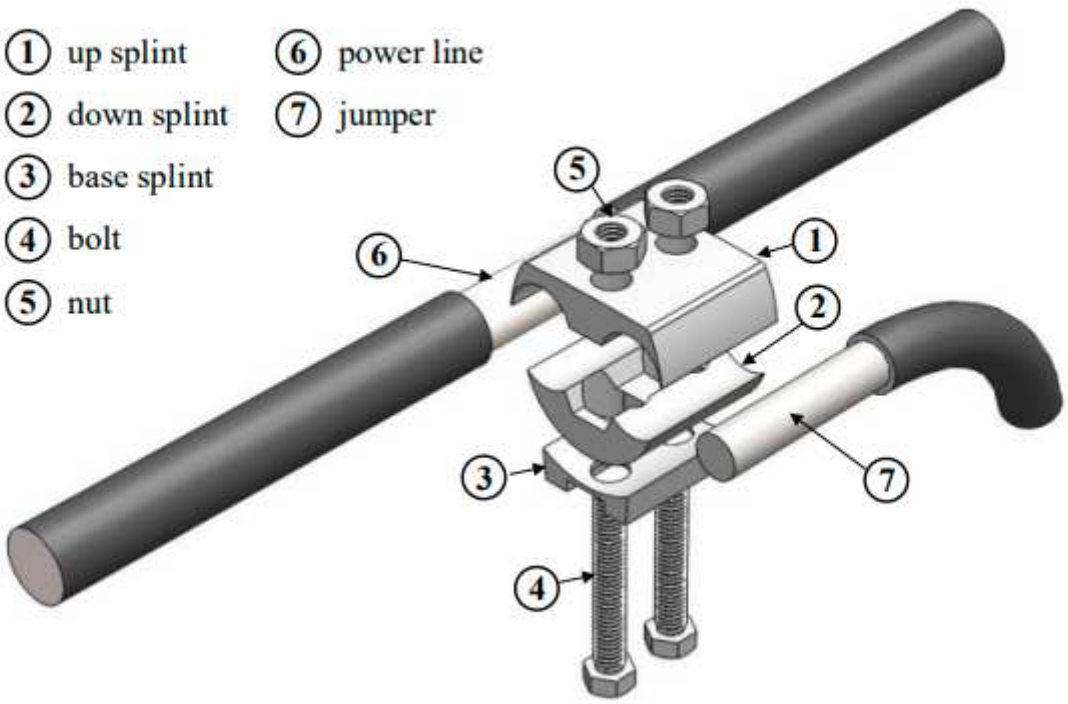

Figure 1

Exploded view of the parallel groove clamp and power line.

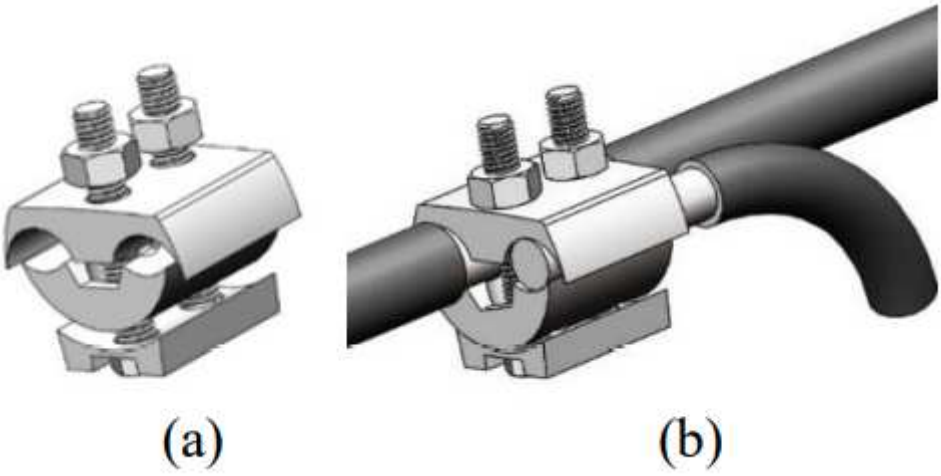

Figure 2

Assembly states of the parallel groove clamp. (a) Initial state; (b) final state.

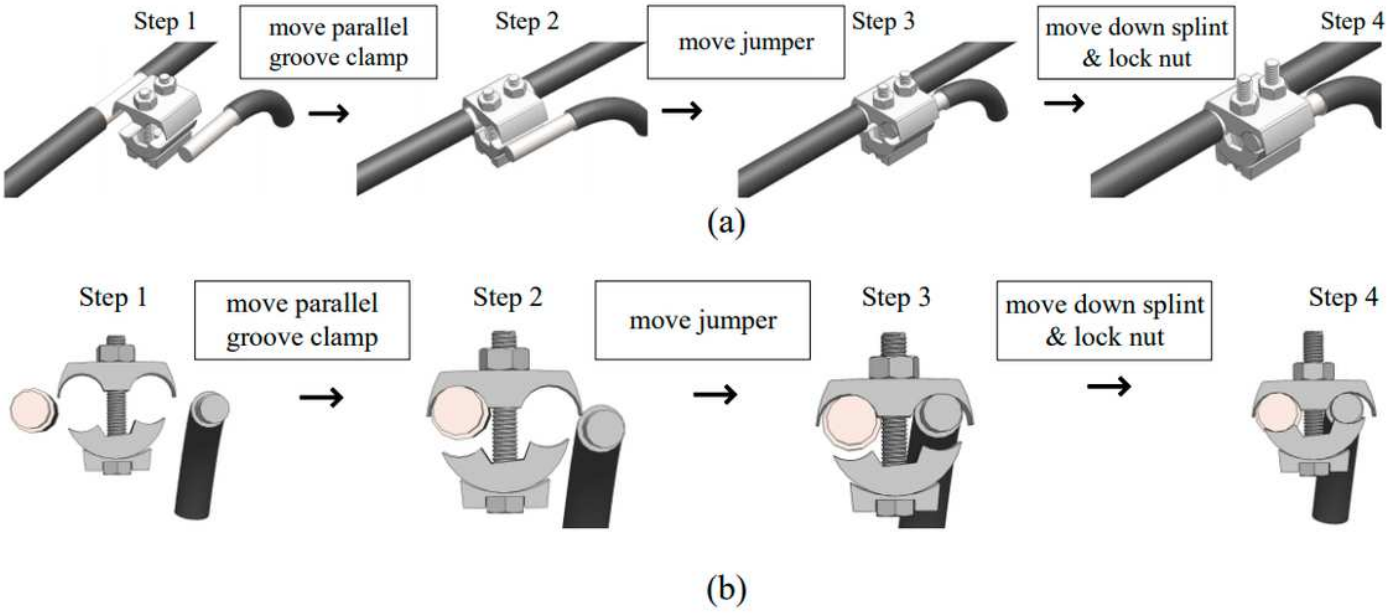

Figure 3

Assembly steps. (a) 3D view; (b) cutaway view.

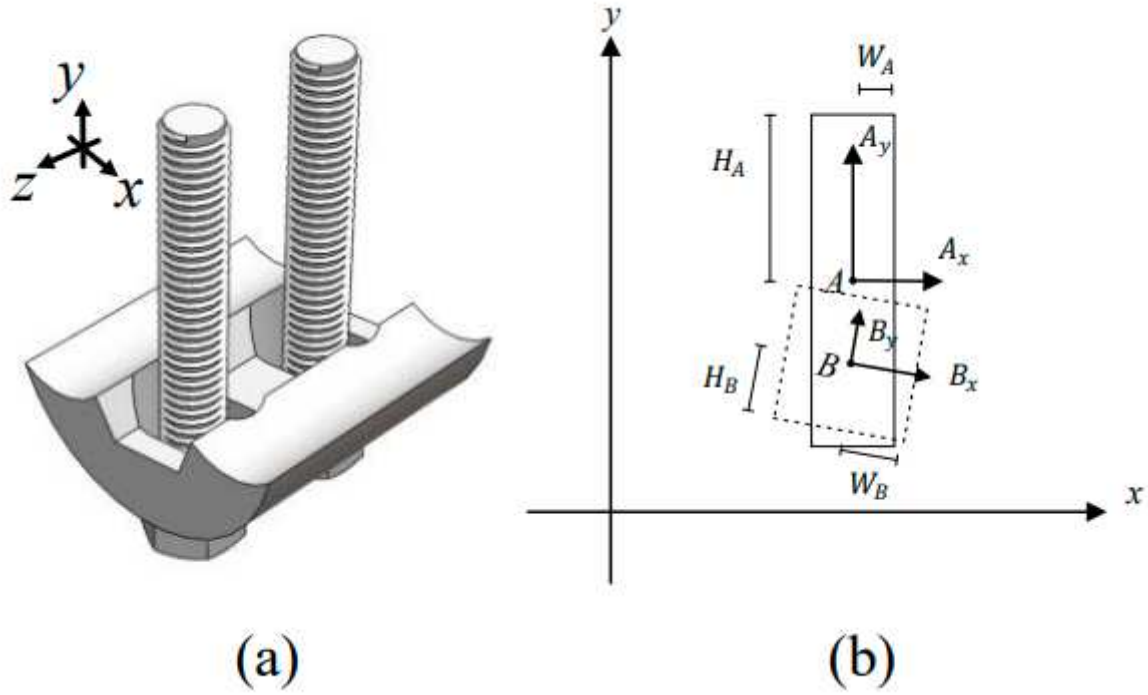

Figure 4

OBB-based collision detection. (a) Down splint collides with bolt; (b) simplified OBB collision.

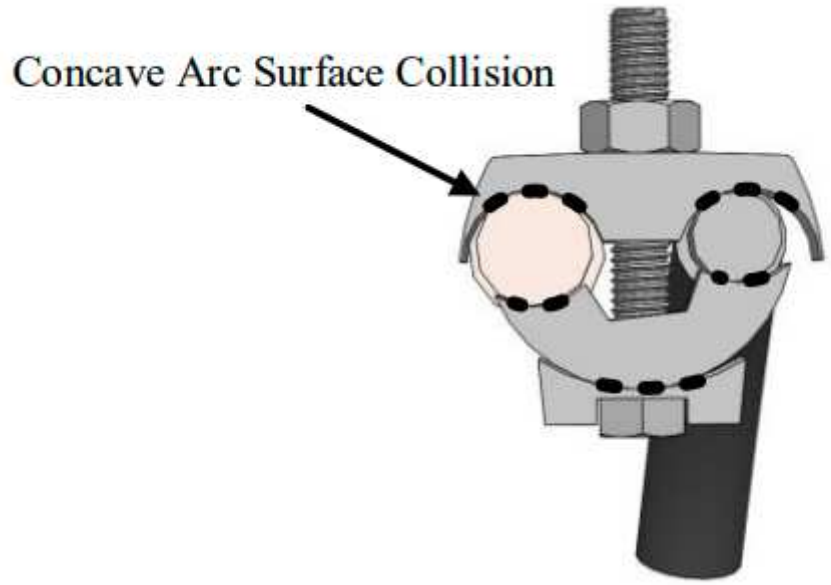

Figure 5

CAS collision cutaway view.

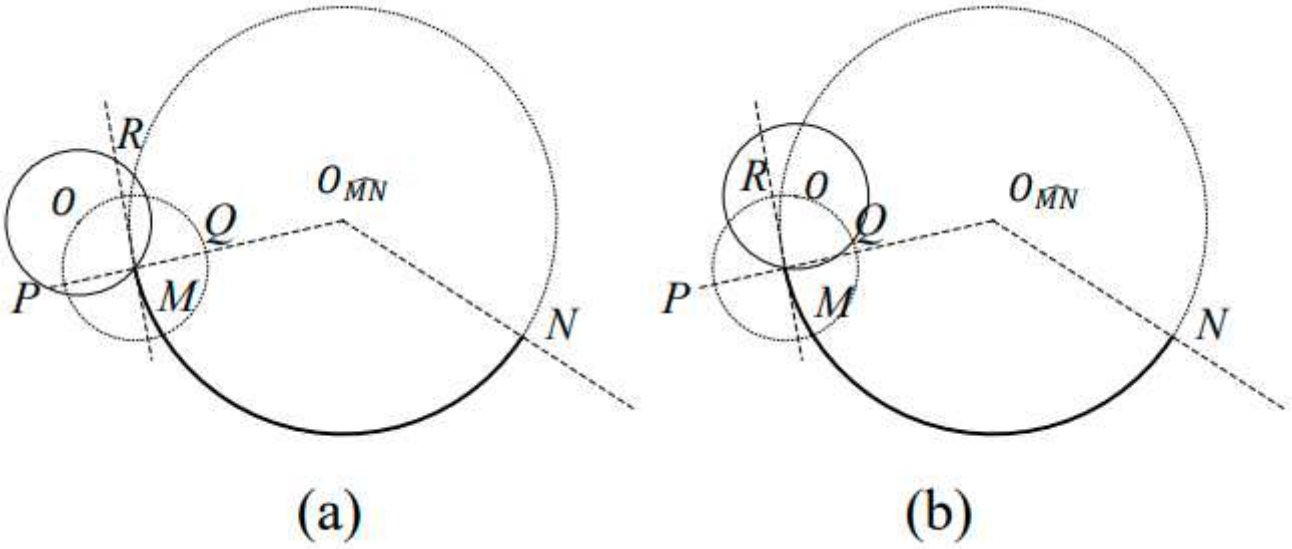

Figure 6

The small circle O contacts arc O_(MN) ⌢ at point M. (a) Exterior contact; (b) interior contact.

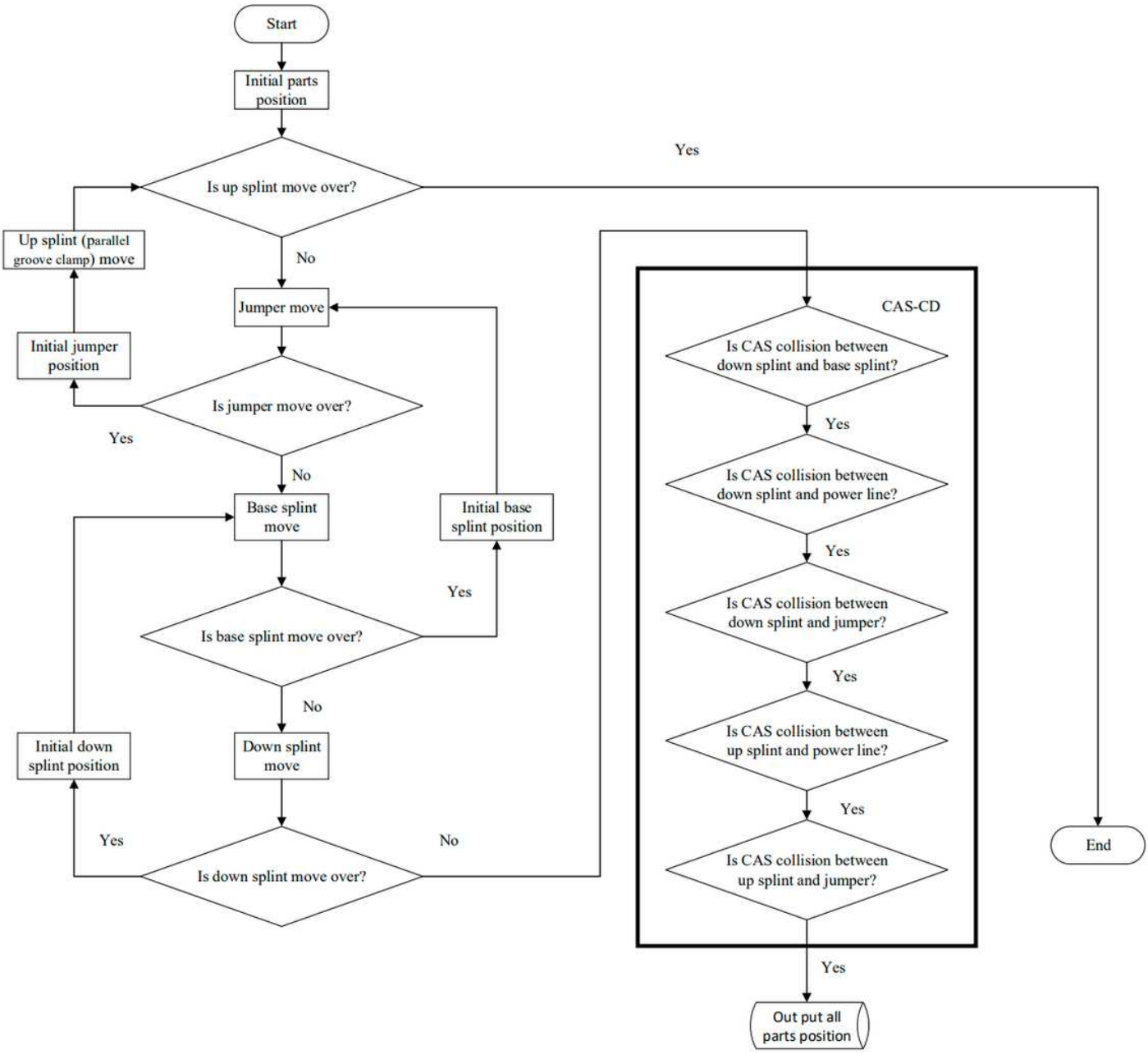

Figure 7

Flow diagram of the virtual movement algorithm of the parallel groove clamp.

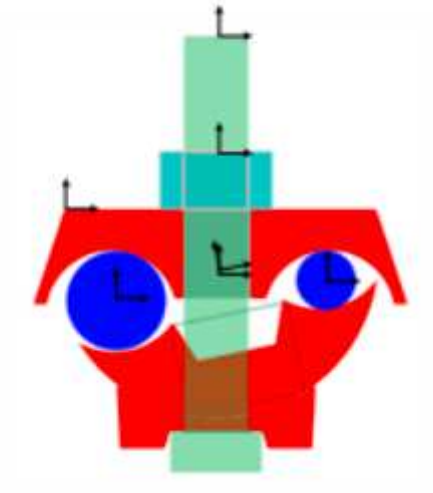

Figure 8

Final state based on CAS-CD.

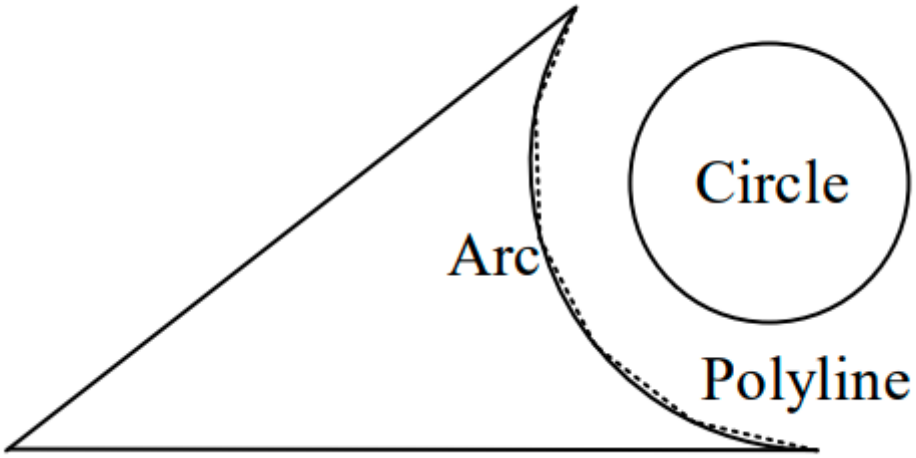

Figure 9

Convex partition.

Figure 10

Image detection.

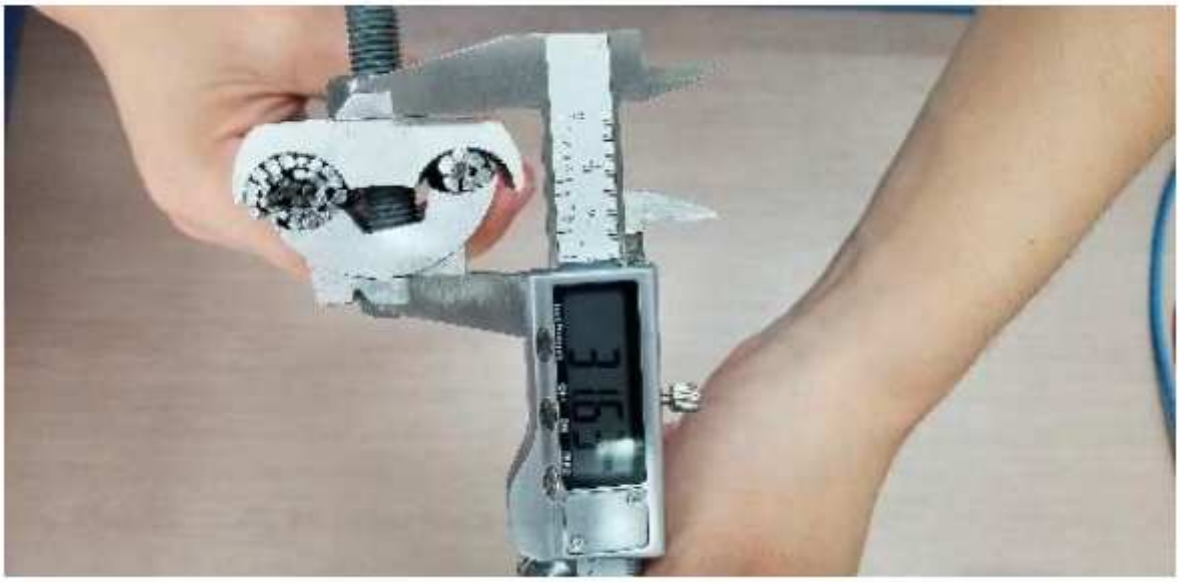

Figure 11

The actual distance.